Published in : Planta Med (2021), vol. 87, n°12-13, pp. 1008–1017
DOI: 10.1055/a-1532-2384
Status : Postprint (Author's version)

CYTOTOXICITY OF POUPARTONE B, AN ALKYL CYCLOHEXENONE DERIVATIVE FROM *POUPARTIA BORBONICA*, AGAINST HUMAN CANCER CELL LINES[#]

Allison Ledoux[1], Daphnée Bériot[2], Lucia Mamede[1], Pauline Desdemoustier[1], Fanny Detroz[1], Olivia Jansen[1], Michel Frédérich[1]*, Erik Maquoi[2]*

[1]*Laboratory of Pharmacognosy, Center of Interdisciplinary Research on Medicines (CIRM), University of Liège, Belgium*
[2]*Laboratory of Tumors and development Biology, GIGA-Cancer, CIRM, University of Liège, Liège, Belgium*

Correspondence: Dr. Allison Ledoux ; Laboratory of Pharmacognosy, University of Liège Avenue Hippocrate 15, 4000 Liège, Belgium ; Phone: + 32 43 66 43 36, Fax: + 32 43 66 43 32 ; allison.ledoux@uliege.be

Supplementary material is available under https://doi.org/10.1055/a-1532-2384

KEYWORDS

Anacardiaceae, *Poupartia borbonica*, poupartone B, cancer, cytotoxicity, live-cell imaging

ABSTRACT

Poupartia borbonica is an endemic tree from the Mascarene Islands that belongs to the Anacardiaceae family. The leaves of this plant were phytochemically studied previously, and isolated alkyl cyclohexenone derivatives, poupartones A-C, demonstrated antiplasmodial and antimalarial activities. In addition to their high potency against the *Plasmodium sp.*, high toxicity on human cells was also displayed. The present study aims to investigate in more detail the cytotoxicity and pharmacological interest of poupartone B, one of the most abundant derivatives in the leaves of *P. borbonica*. For that purpose, real-time live-cell imaging of different human cancer cell lines and normal fibroblasts, treated or not treated with poupartone B, was performed. A potent inhibition of cell proliferation associated with the induction of cell death was observed. A detailed morphological analysis of different adherent cell lines exposed to high concentrations of poupartone B (1-2 µg/mL) demonstrated that this compound induced an array of cellular alterations, including a rapid retraction of cellular protrusions associated with cell rounding, massive cytoplasmic vacuolization, loss of plasma membrane integrity, and plasma membrane bubbling, ultimately leading to paraptosis-like cell death. The structure-activity relation of this class of compounds, their selective toxicity, and pharmacological potential are discussed.

**MF and EM are co-senior authors of this work.*
 # Dedicated to Professor Arnold Vlietinck on the occasion of his 80thbirthday.

Published in : Planta Med (2021), vol. 87, n°12-13, pp. 1008–1017
DOI: 10.1055/a-1532-2384
Status : Postprint (Author's version)

Introduction

Poupartone B is an alkyl cyclohexenone derivative that has been isolated from a Mascarene Island endemic plant, the *Poupartia borbonica* Gmel. A previous study established its antiplasmodial properties on chloroquine-resistant *Plasmodium falciparum* strain W2 and chloroquine-sensitive strain 3D7 [1].

Alkyl cyclohexenone derivatives represent a rare group of secondary metabolites which, as far as it could be established, were reported exclusively in plants in the Anacardiaceae family. However, in 2015, pseudohygrophorones, another set of derivatives of this chemical group, were isolated in the fungal kingdom from *Hygrophorus abieticola* Krieglst. ex Gröger & Bresinsky [2]. A vast array of biological properties have been reported for alkyl cyclohexenone derivatives, including antiplasmodial [1], antibacterial [3], antiphytopathogenic fungi [2], and cytotoxic [4, 5] properties (▸ Table 1 and Fig. 1). Collectively, the data emphasizes the pharmacological potential of these compounds, with a special interest in their cytotoxic properties. However, the lack of detailed toxicological information related to this infrequent class of compounds hampers further therapeutic development. Any additional information about their structure-activity relationships and pharmacological potentialities could prove to be a unique opportunity for the drug discovery process. In this manuscript, we investigated the *in vitro* cytotoxicity of poupartone B on normal human fibroblasts as well as on solid tumorand blood-derived cancer cell lines.

Published in : Planta Med (2021), vol. 87, n°12-13, pp. 1008–1017
DOI: 10.1055/a-1532-2384
Status : Postprint (Author's version)

▶ **Table 1** Plants containing alkyl cyclohexenone derivatives, their structures, their bioactivities, and/or toxicities (structures are depicted in ▶ **Fig. 1**).

Plant	Part	Compounds	Bioactivities investigated	Cytotoxicity (against noncancer cell lines)
Tapirira guianensis [4]	seeds	2-[10(*Z*)-heptadecenyl]-1,4-hydroquinone (**1**) 4,6-Dihydroxy-4-[10(*Z*)-heptadecenyl]-2-cyclohex-enone (**2**)	Cytotoxic activities against **cancer cells**; **BC1**, human breast cancer; **Lu1**, human lung cancer; **Col2**, human colon cancer; **KB**, human epidermoid carcinoma; **LNCaP**, human hormone-dependent prostate cancer (IC_{50} between 0.2–4.3 µg/mL)	–
	bark	4,6,20-Trihydroxy-6-[10(*Z*)-heptadecenyl]-1-cyclohexen-2-one (**3a**); 1,4,6-trihydroxy-1,20-epoxy-6-[10(*Z*)-heptadecenyl]-2-cyclohexene (**3b**) in mixture	Antiparasitic activities against ***P. falciparum***, ***Leishmania amazonensis*** (IC_{50} between 1–5.4 µM); cytotoxic activities against **cancer cells MCF-7** (IC_{50}: 6.8 µM)	–
		1,4,5,20-Tetrahydroxy-1-[10(*Z*)-heptadecenyl]-2-cyclohexene (**4**)	Antiparasitic activities against ***P. falciparum***, ***L. amazonensis*** (IC_{50} between 86.4–95.5 µM); cytotoxic activities against **cancer cells MCF-7** (IC_{50}: 34.8 µM)	–
		1,3,4,6-Tetrahydroxy-1,20-epoxy-6-[10(*Z*)-heptadecenyl]-cyclohexane (**5**)	Antiparasitic activities against ***P. falciparum***, ***L. amazonensis*** (IC_{50} between 86.490.4–159.5 µM); cytotoxic activities against **cancer cells MCF-7** (IC_{50}: 74.1 µM)	–
Tapirira obtusa [5]	bark	**6a**: n = 10; **6b**: n = 8 **7a**: n = 15; **7b**: n = 13 1-Hydroxy-3-[(*Z*)-7H-nonadecenyl]benzene (**6a**); 1-hydroxy-3-[(*Z*)-7H-heptadecenyl]benzene (**6b**); 1- hydroxy-3-heptadecenyl-benzene (**7b**); 1-hydroxy-3- pentadecenylbenzene (**7b**)	Cytotoxic activities against **Lu1**, human lung cancer; **Col2**, human colon cancer; and **LNCaP**, human hormone-dependent prostate cancer (IC_{50} between 15.5–18.8 µg/mL)	–
		8a: n = 13; **8b**: n = 11 1-Hydroxy-3-[14H-phenyltetradecyl]benzene (**8a**);1-hydroxy-3-[14H-phenyldodecyl]benzene (**8b**)	Cytotoxic activities against **cancer cells KB**, human epidermoid carcinoma (IC_{50}: 14.4 µg/mL)	–
		1-(16H-Phenyl-12H-(*Z*)-hexadecenyl)- 4-cyclohexene- (1S*,3S*)-diol (**9**)	Cytotoxic activities against **cancer cells Lu1**, human lung cancer; **Col2**, human colon cancer; **KB**, human epidermoid carcinoma (IC_{50} between 10.2–19.5 µg/mL)	–
		4S*, 6S*-Dihydroxy-6-(14H-nonadecenyl)2-cyclo- hexenone (**10**)	Cytotoxic activities against **cancer cells**; **BC1**, human breast cancer; **Lu1**, human lung cancer; **Col2**, human colon cancer; **KB**, human epidermoid carcinoma; **LNCaP**, human hormone-dependent prostate cancer (IC_{50} between 1–12 µg/mL)	–
Poupartia borbonica [1]	Leaves	Poupartone A (**11**) Poupartone B (**12**) Poupartone C (**13**)	Antiparasitic activities against ***P. falciparum***, (IC_{50} between 0.55–1.81 µM) Cytotoxic activities against **cancer cells (HeLa)**, (IC_{50} between 2.10–3.77 µM)	**WI-38** cells (IC_{50} between 1.58–2.66 µM)

continued

Plant	Part	Compounds	Bioactivities investigated	Cytotoxicity (against noncancer cell lines)
Lannea rivae [6, 7]	Root stem	**14a**: n = 10; **14b**: n = 8; **14c**: n = 6 **14d**: n = 10 3-[nonadec-14(*Z*)-enyl]-phenol (**14a–d**) in mixture	No antibacterial nor antiparasitic activities *(Enterococcus faecalis, Staphylococcus aureus, Escherichia coli, Pseudomonas aeruginosa, P. falciparum)*	No cytotoxicity Chinese hamster ovarian cell (CHO) (IC_{50} > 100 µg/mL)
		15: n = 10 4,5-dihydroxy-4,5-furan-20-[16(*Z*),18(E)-non adecadienyl]-cyclo-hex-2-enone (**15**)	Antiparasitic activities against ***P. falciparum***, (IC_{50} between 0.43–0.48 µg/mL) Antibacterial activities against ***E. faecalis, S. aureus, E.coli, P. aeruginosa***	CHO (IC_{50} = 1.93 µg/mL)
		16: n = 12 2,4,5-trihydroxy-2-[heneicos-16(*Z*)-enyl]-cydohex-anone (**16**)	Antiparasitic activities against ***P. falciparum***, (IC_{50} between 1.40–2.05 µg/mL)	CHO (IC_{50} = 6.52 µg/mL)
		17a: n = 8; **17b**: n = 10 4S,6R-dihydroxy-6-[12(*Z*)-heptadecenyl]-cyclo-hex-2-enone (**17a–b**) in mixture	**Antiparasitic activities against *P. falciparum***, (IC_{50} between 0.88–1.03 µg/mL) Antibacterial activities against ***E. faecalis, S. aureus, E.coli, P. aeruginosa*** (zones of inhibition in mm between 8–16)	**No cytotoxicity** CHO (IC_{50} > 100 µg/mL)
		18: n = 12 1,2,4-trihydroxy-4-[16(*Z*)-heneicosenyl]-cyclohex-ane (**18**)	No antibacterial nor antiparasitic activities *(E. faecalis, S. aureus, E.coli, P. aeruginosa; P. falciparum)*	CHO (IC_{50} = 56.5 µg/mL)
		(4R,6S)-4,6-Dihydroxy-6-((*Z*)-nonadec-14′-en-1-yl)cyclohex-2-en-1-one (**19**)	**Antibacterial activities** against ***E.coli*** (zones of inhibition in mm: 9 at 150 µg/mL; 59.44% of inhibition with 80 µg/mL) Cytotoxic activities against **cancer cells (DU-145)**, (IC_{50} = 0.55 µg/mL)	No cytotoxicity Vero cells (IC_{50} > 100 µg/mL)
		(2S*,4R*,5S*)-2,4,5-Trihydroxy-2-((*Z*)-nonadec-14′-en-1-yl)cyclo-hexanone (**20**)	Antibacterial activities against ***S. aureus***, (59.44% of inhibition with 80 µg/mL) Not active against *E. coli*	–
Fungi	**Part**	**Compounds**	**Bioactivities**	**Toxicity**
Hygrophorus abieticola [2]		Pseudohygrophorone A^{12} (**21**) Pseudohygrophorone B^{12} (**22**) Hygrophorone B^{12} (**23**)	Fungicidal plant protection agent: antiphytopathogenic activities against *Botrytis cinerea*, *Septoria tritici*, and *Phytophthora infestans* (IC_{50} between 1.6–24.5 µM)	–

Published in : Planta Med (2021), vol. 87, n°12-13, pp. 1008–1017
DOI: 10.1055/a-1532-2384
Status : Postprint (Author's version)

Published in : Planta Med (2021), vol. 87, n°12-13, pp. 1008–1017
DOI: 10.1055/a-1532-2384
Status : Postprint (Author's version)

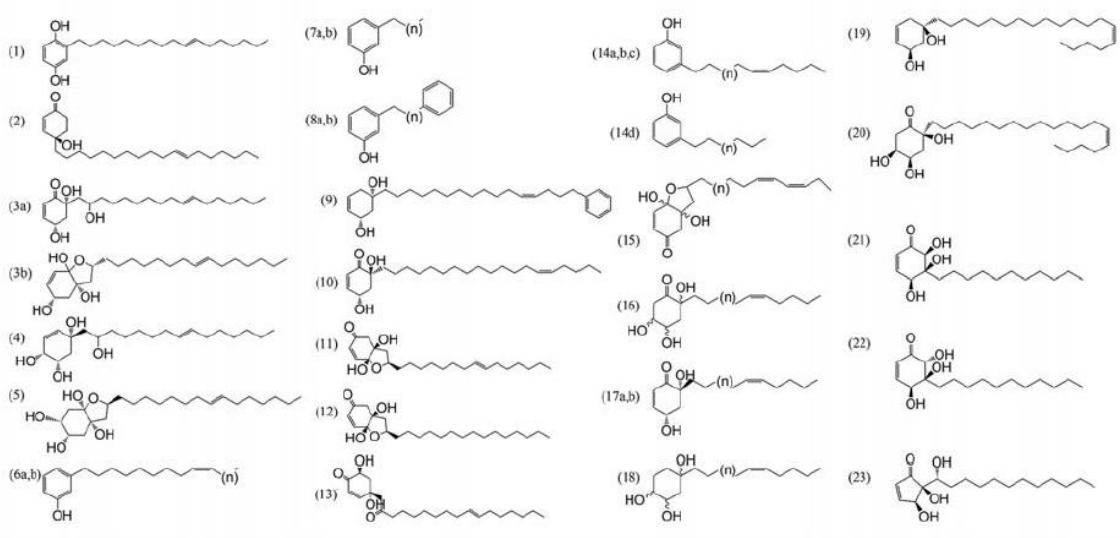

▶ Fig. 1 Structures of compounds described in ▶ Table 1.

Results

The potential influence of poupartone B on the behavior of human cancer cell lines and normal fibroblasts was investigated by using live-cell imaging. Three adherent cancer cell lines (a triple-negative breast adenocarcinoma cell line MDA-MB-231, and 2 metastatic melanoma cell lines: A2058 and A375) and normal adult human skin fibroblasts were used.

As high cell density within an individual population can alter sensitivity to death-inducing stimuli [8, 9], cells were seeded so that they were less than 50 % confluent when first exposed to treatments. To validate our cytotoxicity assay, MDA-MB-231 cells were treated for 48 h with increasing concentrations (0.02 to 200 µM) of etoposide, a well-described chemotherapeutic drug [10-11].

Following the addition of increasing concentrations of poupartone B (0-2 µg/mL), adherent cells within each population were analyzed by live-cell imaging microscopy for 48 h, except for fibr blasts, which were imaged for 80 h due to their lower proliferative capacity. Phase-contrast images were acquired every hour to assess population confluence and morphology. Treatment with vehicle (DMSO 0.5 %) was not lethal to either cell line, and the surface area covered by cells increased exponentially during the 48h of treatment (▸ Fig. 2). When used at low concentrations (0.12 to 0.50 µg/mL), poupartone B had a limited influence on the proliferation of the MDA-MB-231, A2058, and A375 cancer cell lines (▸ Fig. 2 a-c). Normal fibroblasts displayed a slightly higher sensitivity to these low poupartone B concentrations when compared with cancer cell lines (▸ Fig. 2 d). In contrast, the 2 highest poupartone B concentrations tested (1-2 µM) strongly impaired the proliferation of the 4 adherent cell lines (▸ Fig. 2). Morphological analysis of time-lapse phase contrast images revealed that poupartone B affected cell morphology in a time and concentration-dependent manner. While vehicle-treated cells displayed a normal morphology characterized by a flat cytoplasm with active lamellipodial and pseudopodial extensions (▸ Fig. 3), poupartone B treatment (1-2 µg/mL) induced a rapid retraction of the cytoplasmic extensions, leading to cell rounding (▸ Fig. 3 and Fig. 1S-4S, Supporting Information). Exposure of cells to poupartone B (2 µg/mL) for 6 h was sufficient to induce rounding in almost all cancer cells (Fig. 1S-3S, Supporting

Published in : Planta Med (2021), vol. 87, n°12-13, pp. 1008–1017
DOI: 10.1055/a-1532-2384
Status : Postprint (Author's version)

Information). In contrast, complete rounding of fibroblasts required a longer exposure time (about 24 h, Fig. 4S, Supporting Information).

A detailed observation of the 4 cell lines revealed that cell rounding was followed by cell death. The nonviable cells were characterized by cytoplasmic swelling and plasma membrane bubbles (▸ Fig. 3, *white arrowheads*). Loss of plasma membrane integrity was also investigated by including YOYO-3 (a cell-impermeant dye that stains double-stranded DNA) in the growth medium of MDA-MB-231 and A375 cells. As shown in ▸ Fig. 4,a high percentage of blebbing cells observed in the presence of high concentrations of poupartone B displayed a red nuclear fluorescence, confirming the loss of plasma membrane integrity. Red fluorescence was also observed in some plasma membrane bubbles, suggesting a release of the nuclear content into the cytoplasm of these dying cells. However, apoptotic-like morphologies characterized by the presence of specific membrane protrusions (apoptopodia) were observed in a fraction of the 3 cancer cell lines exposed to high concentrations of poupartone B (data not shown). In contrast, dead cells were seldomly observed in vehicle-treated cultures (▸ Fig. 3 and Fig. 1S-4S, Supporting Information).

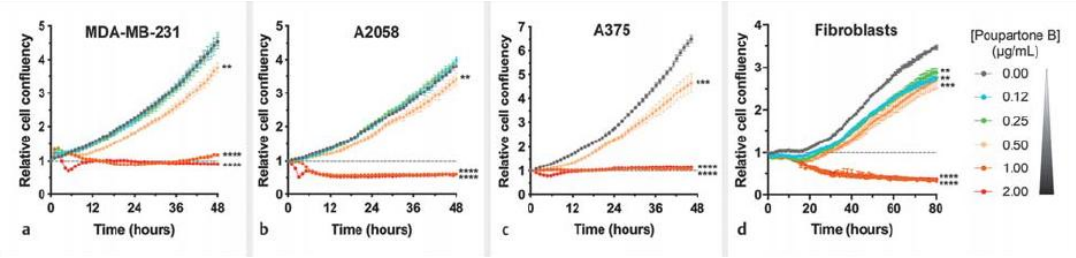

▶ Fig. 2 Effect of poupartone B on cell growth. Adherent (a) MDA-MB-231, (b) A2058, (c) A375, and (d) fibroblasts cell lines were treated with increasing concentrations (0.12-2 µg/mL) of poupartone B or vehicle only for 48 (a, b, c) or 80 (d) h. Live-cell imaging was used to measure the cell confluency (relative to time 0). Data are presented as mean ± SEM (n = 3 wells/experiment). A representative experiment is illustrated. Kolmogorov- Smirnov test: ** $p < 0.01$; *** $p < 0.001$; ****0 $p < 0.0001$.

Published in : Planta Med (2021), vol. 87, n°12-13, pp. 1008–1017
DOI: 10.1055/a-1532-2384
Status : Postprint (Author's version)

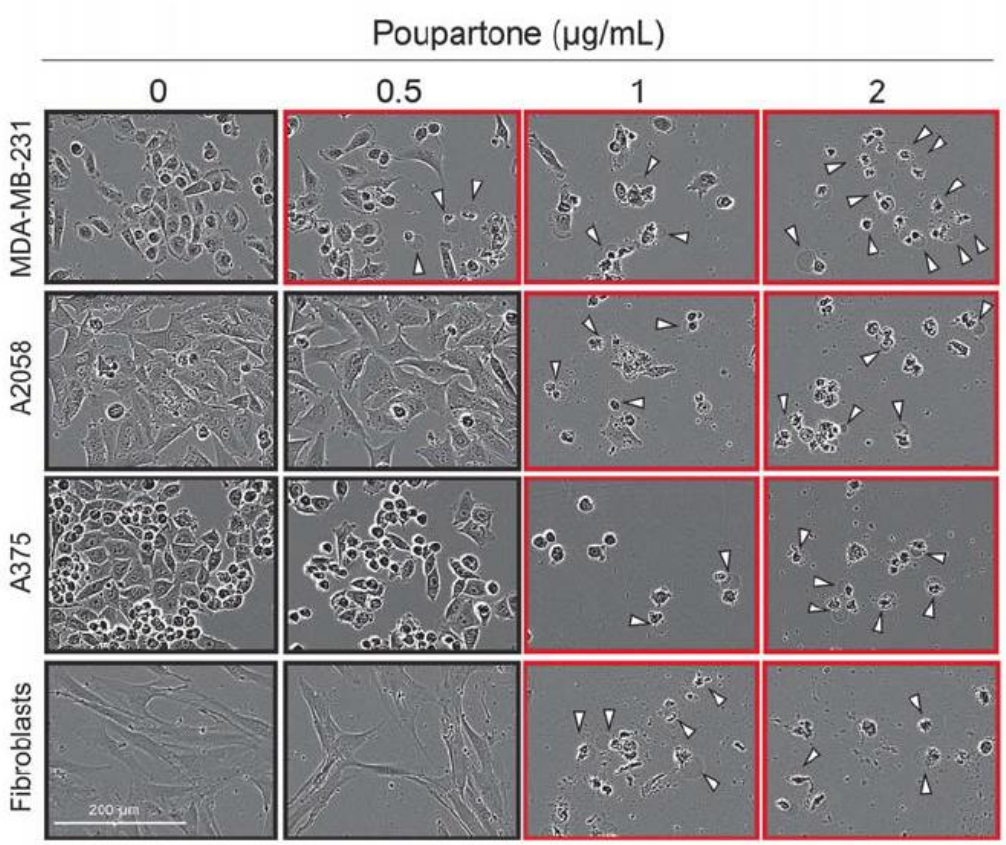

▶ Fig. 3 Influence of poupartone B on cell morphology. Representative phase-contrast images of adherent (MDA-MB-231, A2058, A375, and fibroblasts) cells treated for 48 h with increasing concentrations of poupartone B or vehicle. White arrowheads indicate dead cells. Images con- taining dead cells are marked by a red border. Scale bar = 200 µm.

To analyze in more detail the morphological alterations induced by our compound of interest, MDA-MB-231 cells were exposed for 12 h to poupartone B (1 µg/mL) and imaged by holotomographic microscopy. This method allows live imaging of the major cellular structures without the need to label the cells. In agreement with the low-resolution phase-contrast images (▸ Fig. 3 and Fig. 1S–4S, Supporting Information), the holo-tomographic data (supplementary video), confirmed that cell response to poupartone B treatment was heterogeneous, with some cells remaining unaffected while others displayed strongly altered morphologies. The earliest alteration observed was a time-dependent contraction of cell protrusions, resulting in a progressive rounding of the cells (▸ Fig. 5 a and supplementary video). The second major morphological alteration required a longer exposure to poupartone B (about 6 h) and consisted in the pro gressive appearance of multiple perinuclear vacuoles. Once initiated, cytoplasmic vacuolization progressed rapidly and led to cell compaction and subsequent death (▸ Fig. 5 b and supplementary video). In contrast, no significant alteration of the nuclear organization was detected in any of the observed cells (▸ Fig. 5 a, b and supplementary video). These morphological observations suggest the occurrence of a paraptosis-like cell death characterized by and a diffuse large B-cell lymphoma, respectively) were used.

Published in : Planta Med (2021), vol. 87, n°12-13, pp. 1008–1017
DOI: 10.1055/a-1532-2384
Status : Postprint (Author's version)

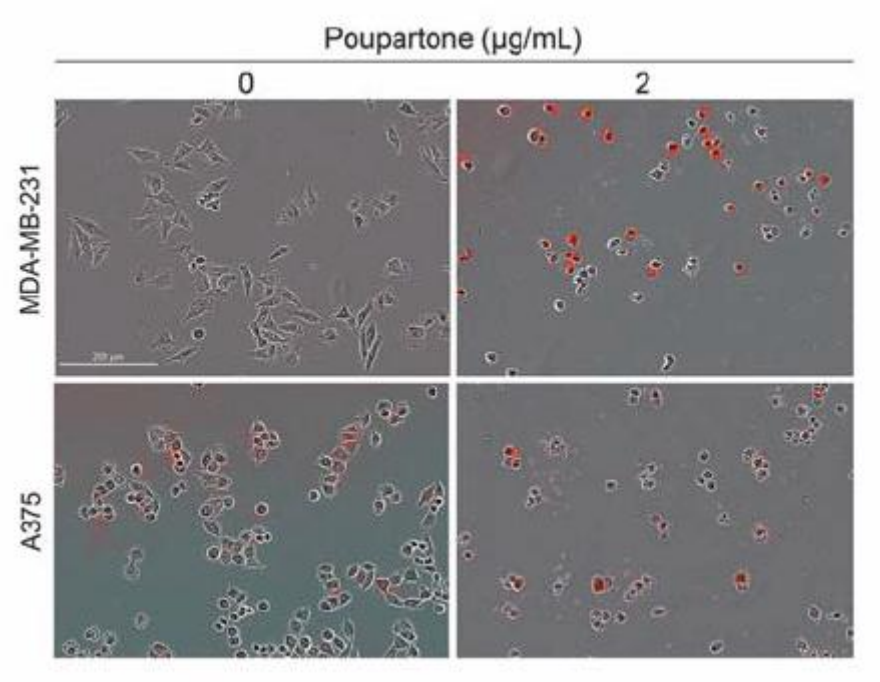

► Fig. 4 Poupartone B impairs plasma membrane integrity. Repre- sentative phase-contrast images of MDA-MB-231 and A375 cells treated for 12 h with poupartone B (2 µg/mL) or vehicle in the presence of YOYO-3. Red fluorescence specifically labels cells with a permeant plasma membrane. Scale bar = 200 µm.

A preliminary dose-response experiment indicated that these 2 cell lines were more sensitive to poupartone B treatment than the adherent ones, with a complete inhibition of cell growth observed from 0.5 µg/mL (data not shown). Live-cell imaging analysis demonstrated that poupartone B induced a strong reduction of cell confluency when used at concentrations ≥ 0.25 µg/mL (► Fig. 6 a, b). This inhibition of cell growth was associated with a striking increase of dead cells. Most dying cells were characterized by the formation of a single blister (► Fig. 6 c).

Published in : Planta Med (2021), vol. 87, n°12-13, pp. 1008–1017
DOI: 10.1055/a-1532-2384
Status : Postprint (Author's version)

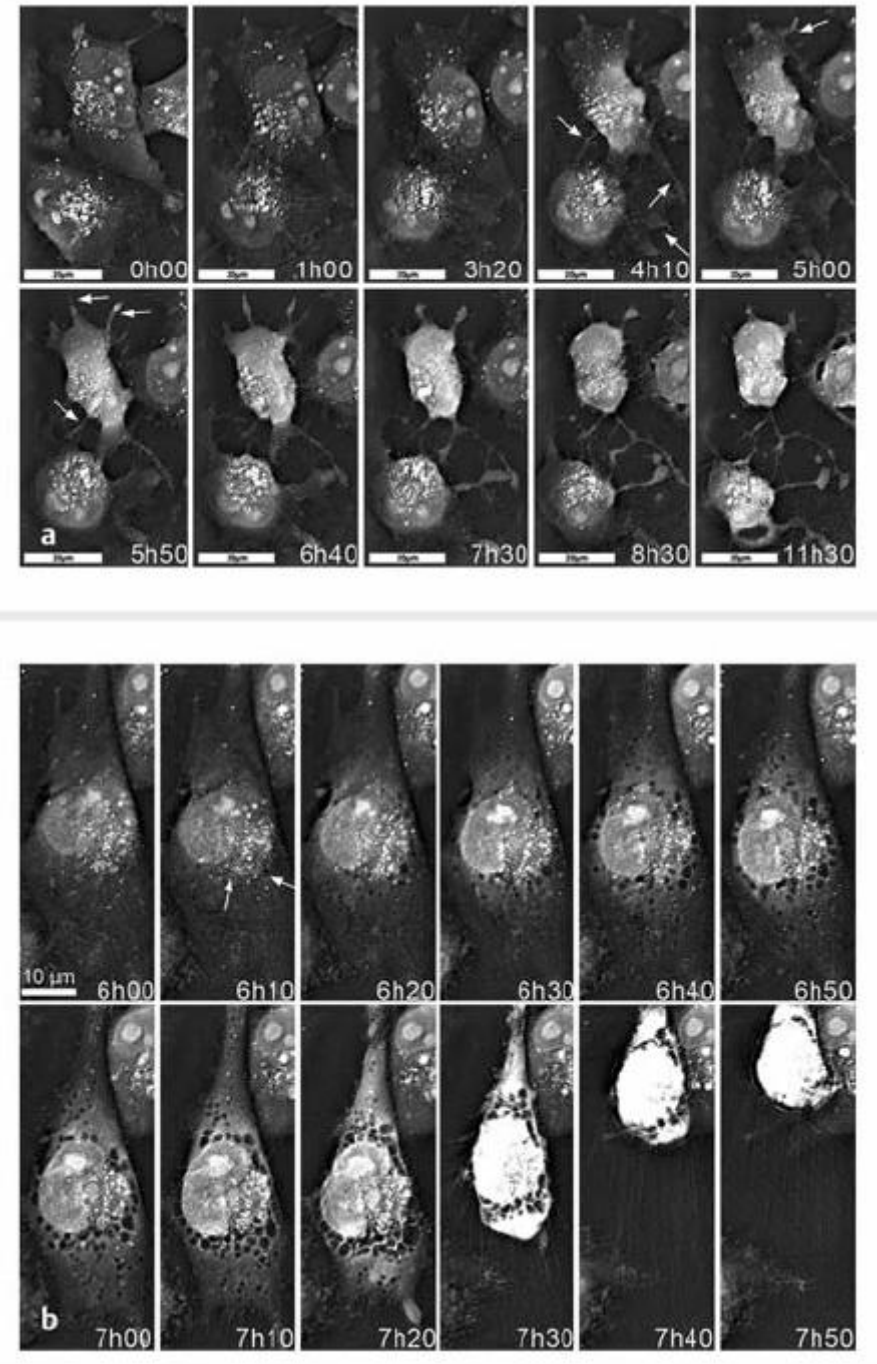

► Fig. 5 Holo-tomographic microscopy of poupartone B-treated MDA-MB-231 cells. MDA-MB-231 cells were exposed to poupartone B (1 µg/mL), and time-lapse imaging by holo-tomographic micros- copy was performed for 13 h. Representative images illustrating (a) the progressive contraction of cytoplasmic protrusions (white arrows) and (b) the evolution of cytoplasmic vacuoles (white arrows) are shown. Scale bar = 20 µm.

Collectively, these different results support the hypothesis that poupartone B is a potent cytotoxic molecule that displays a slight selectivity towards blood cancer-derived cell lines. The comparison of IC_{50} values (► Table 2) on the different cell lines investigated in this study revealed that poupartone B is about 3 times more active on blood-derived cancer cells as compared to solid tumor-derived cells and normal fibroblasts. Representative dose-response curves for the 6 cell lines investigated are illustrated in Fig. 5S (Supporting Information).

Published in : Planta Med (2021), vol. 87, n°12-13, pp. 1008–1017
DOI: 10.1055/a-1532-2384
Status : Postprint (Author's version)

Discussion

In the present study, *in vitro* assays were performed on different human cancer cell types, including triple-negative breast cancer (MDA-MB-231), 2 metastatic melanomas (A2058 and A375), acute promyelocytic leukemia (HL-60), and diffuse large B-cell lymphoma (OCI-LY19), as well as on normal fibroblasts to better decipher the cytotoxic activity of poupartone B, an alkyl cyclo hexenone derivative endowed with antiplasmodial and antimalarial activities.

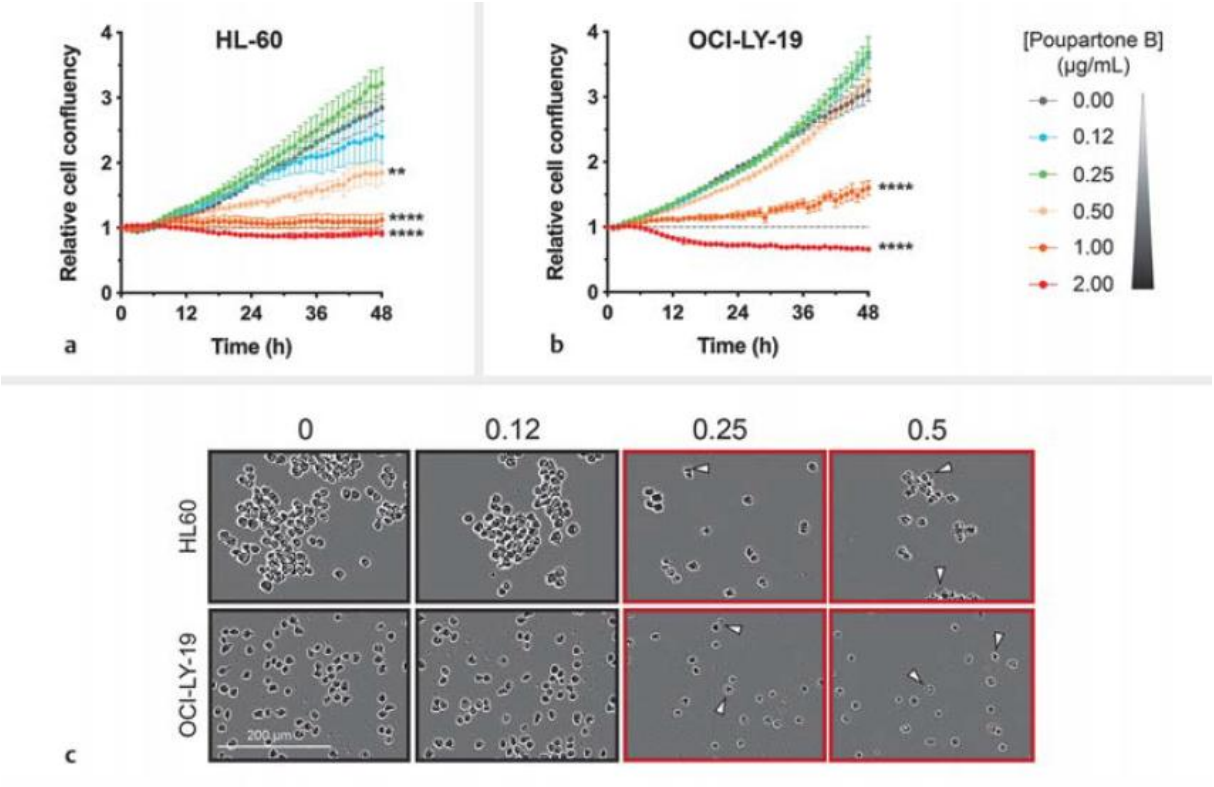

► Fig. 6 Effect of poupartone B treatment on nonadherent cell lines. HL-60 and OCI-LY19 cells were treated with increasing concentrations (0.03–0.5 µg/mL) of poupartone B or vehicle for 48 h. a, b Live cell imaging was used to measure the cell confluency (relative to time 0). Data are presented as mean ± SEM (n = 3 wells/experiment). A representative experiment is illustrated. Kolmogorov-Smirnov test: ** $p < 0.01$; **** $p < 0.0001$. c Influence of poupartone B on cell morphology. Representative phase-contrast images of HL-60 and OCI-LY19 cells treated for 48 h with increasing concentrations of poupartone B or vehicle. White arrowheads indicate dead cells. Images containing dead cells are marked by a red border. Scale bar = 200 µm.

This compound inhibits the proliferation of the different cell types investigated with a 3-fold higher potency toward blood-derived cancer cell lines. This inhibition of cell proliferation was shown to be associated with the induction of cell death. A detailed morphological analysis of different adherent cell lines exposed to high concentrations of poupartone B (1–2 µg/mL) demonstrated that this compound induces an array of alterations, including a rapid contraction of cellular protrusions associated with cell rounding, massive cytoplasmic vacuolization, loss of plasma membrane integrity, and plasma membrane bubbling, ultimately leading to cell death. It should be noted that these different morphological alterations do not occur to the same extent and with the same kinetic in all the cell lines tested. For example, while a 12 h exposure to poupartone B was sufficient to induce extensive cell

Published in : Planta Med (2021), vol. 87, n°12-13, pp. 1008–1017
DOI: 10.1055/a-1532-2384
Status : Postprint (Author's version)

rounding and cell death in the 3 adherent cancer cell lines (MDA-MB-231, A2058, and A375) tested, normal fibroblasts remained weakly affected. Even if our morphological data do not allow us to identify with certainty the mode of cell death induced by poupartone B, our observations suggest that at least in some cancer cell lines, such as the triple-negative breast carcinoma MDA-MB-231 cell, paraptosis-like cell death is triggered. Paraptosis is a programmed mode of cell death that is accompanied by the dilation of the ER and/or mitochondria [12]. Various natural products have been reported to induce cytotoxic effects by inducing paraptosis-associated cell death [14]. More investigations will be required to decipher the exact mode(s) of cell death triggered upon poupartone B exposure.Increased apoptosis resistance and insensitivity to therapeutic drugs represent major roadblocks to the effective treatment of several cancers [15–17]. In that context, it is essential to develop new strategies that can induce alternative cell death modes, including paraptosis, whose regulatory mechanisms differ from those of apoptosis, thereby overcoming drug resistance. Through its capacity to induce nonapoptotic cell death, poupartone B might thus represent a useful therapeutic drug to bypass apoptosis resistance.

To the best of our knowledge, this is the first time an alkyl cyclohexenone derivative was tested against blood-derived cancer cells. Our data reveal that these cells are 3 times more sensitive to poupartone B treatment than solid tumor-derived cells, suggesting the interest for this class of compounds as potential chemotherapeutic drugs to fight against these pathologies.

Learning about the toxicity of these kinds of compounds is essential, as their bioactivities are increasingly in the spotlight. The overview of the alkyl cyclohexenones compounds (Table 1) suggests that the toxicity appears to be related to the number of oxygen atoms. However, major biological activities, such as antiplasmodial or cytotoxic, seem to depend on the presence of the α-β unsaturated ketone, a Michael acceptor that is often involved in biological activities. Indeed, as far as it could be established, all the alkyl cyclohexenone derivatives from nature with interesting bioactivities also present a ketone function (compounds 3a, 3b,11, 12, 13, 15, 16, 17a, 17b, and 19) (▸ Fig. 1). The only 2 compounds that demonstrated high bioactivities (antibacterial and cytotoxic) without toxicity to noncancer cell lines contain only 3 oxygen atoms (compounds 17a-b and 19, ▸ Fig. 1), including the α-β unsaturated ketone.

Alkyl cyclohexenone derivatives are a very promising class of compounds with a large panel of biological activities. Some of them demonstrated cytotoxic properties against different type of cells (breast, lung, colon, epidermoid carcinoma, prostate, cervical) as well as antiparasitic activities against *P. falciparum*, the *Plasmodium* species responsible for the most aggressive malaria, and against *Leishmania amazonensis*, one of the parasites responsible for the disease leishmaniasis. Some showed interesting antibacterial activities both against positive and negative gram bacteria, even antifungal activities. Additional structure-activity studies targeting these activities should be performed to confirm the link between toxicity and the number of oxygen atoms in these molecules. If confirmed, it would suggest that it might be possible to decrease overall toxicity by modifying this number, while maintaining other pertinent activities. Additionally, if their activity is proven to be related to the α-β unsaturated ketone, then alkyl cyclohexenones could serve as the basis structure for the development of innovative anticancer, antiparasitic, and antifungal drugs. This study paves the way for further investigations with this compound group to define clearly the mechanism of toxicity and encourage hemi-synthesis or total synthesis to obtain a similar structure, preserving the α-β unsaturated ketone part and a reduced number of oxygen atoms, and evaluate their impact activity-wise.

Published in : Planta Med (2021), vol. 87, n°12-13, pp. 1008–1017
DOI: 10.1055/a-1532-2384
Status : Postprint (Author's version)

Material and Methods

PLANT MATERIAL

The leaves of *P. borbonica* were collected on Reunion Island and were identified by H. Thomas (Parc National de la Réunion). Voucher specimens (no. RUN 028F, TPN-P022F) were deposited in the Herbarium of the University of Reunion Island. Poupartone B was isolated from the leaves of *P. borbonica*, as previously described by our team. Briefly, the defatted crude EtOAc extract was submitted to an open silica column, eluting with a gradient of EtOAc and CH_2Cl_2 from 5 : 95 to 100 : 0. The active fraction containing poupartone B was purified by preparative HPLC with an HPLC column (30 cm × 2.5 cm) using a LichroPrep RP-18 (25– 40 µm, Merck) support and a binary solvent system of formic acid 0.1 % in H_2O and MeOH (40 : 60 to 0 : 100 v/v in 30 min) [1].

CELL LINES

Human MDA-MB-231, A2058, and A375 cancer cell lines and human dermal fibroblasts (kindly provided by Dr. A. Colige, Laboratory of Connective Tissues, ULiège) were maintained in high glucose DMEM supplemented with 10 % (v/v) FBS, 100 IU/mL penicillin, 100 µg/mL streptomycin, 1 mM sodium pyruvate, and 2 mM glutamine. Nonadherent HL-60 and OCI-LY19 cell lines were cultured in RPMI 1640 medium supplemented with 10 % (v/v) FBS, 100 IU/mL penicillin, 100 µg/mL streptomycin, and 1 mM sodium pyruvate. Cell lines were obtained from the ATCC. All culture reagents were purchased from Invitrogen. Cultures were maintained in humidified tissue culture incubators (Hera cell, Thermo Scientific) at 37 °C with 5 % CO_2 and 95 % air. All cultures were mycoplasma free as confirmed by the MycoAlert detection kit (Lonza).

CELL SEEDING AND COMPOUND ADDITION

Experiments were performed on 96-well plates. On day 1, cells grown in 10 cm standard tissue culture dishes (Falcon, Becton-Dickinson) were trypsinized and counted using a Cedex XS cell analyzer (Roche Innovatis). One-hundred µL of cell suspension containing 2000 MDA-MB-231, 1250 A2058, or 1500 A375 viable cells were added manually to 96-well tissue culture plates (Falcon, Becton-Dickinson) and grown overnight. For nonadherent cell lines (HL-60 and OCI-LY19), cells were seeded on day 0 in poly-L-ornithine (Sigma) coated 96-well plates (4000 cells/well).

On day 0, vehicle (DMSO) and test compounds were prepared in a growth medium as 3-fold concentrated solutions, and 50 µl of these solutions were added to the cell cultures (final DMSO concentration 0.5 %). Etoposide (Sigma), a chemotherapeutic drug, was used as a positive control. In some experiments, 200 nM YOYO-3 iodide (Thermo Fisher Scientific), a red fluorescent cellimpermeant, high-affinity nucleic acid stain used to label dead cells, was added in the growth medium.

ACQUISITION OF POPULATION IMAGES

Cell population images were obtained over time using an IncuCyte S3 dual-color live content imaging system (Essen BioSciences) residing within an In-VitroCell ES NU-5831 (NuAir) tissue culture incubator

Published in : Planta Med (2021), vol. 87, n°12-13, pp. 1008–1017
DOI: 10.1055/a-1532-2384
Status : Postprint (Author's version)

maintained at 37 °C with 5 % CO_2. Images were acquired using a 10× objective lens in phase contrast, green (Ex: 440-480/Em: 504-544) and red (Ex: 565-605/Em: 625-705)

fluorescence channel. Four images were acquired from each well every 30-120 min for a maximum of 80 h. All IncuCyte experiments were performed at least in triplicate.

LIVE CELL IMAGING AND CONFLUENCE MEASUREMENTS

Automated image analysis routines were optimized for each cell line using the IncuCyte S3 software package and training data from the vehicle and compound-treated samples. Confluency of the cultures was measured using the IncuCyte Confluence software, which quantified cell surface area coverage as confluence values. Relative cell confluency measures, expressed as a ratio relative to time 0, were then analyzed further on Excel (Microsoft) and GraphPad Prism 7.0. Values more than 1.5-fold different from the one immediately preceding in the time course were censored. The observed distribution of the 2 groups was compared by using the Kolmogorov-Smirnov test in Prism 7. P-values lower than 0.05 were considered significant. Quantitative analysis of the effect of drug treatments over time was provided by determining half inhibitory concentration (IC_{50}) calculated using nonlinear regression (4-parameters) from the area under the curve (AUC) values derived from each proliferation profile in GraphPad Prism 7.0.

HOLO-TOMOGRAPHIC MICROSCOPY

Holo-tomographic microscopy (HTM) was performed on a 3D Cell-Explorer Fluo (Nanolive) using a 60× air objective (NA = 0.8) at a wavelength of λ = 520 nm (Class 1 low power laser, sample exposure 0.2 mw/mm^2). This microscope is equipped with a top-stage incubator (Oko-lab), allowing a constant temperature of 37 °C, an air humidity saturation and a CO_2 level of 5 % throughout the acquisitions. MDA-MB-231 cells were seeded in glass-bottom 35-mm culture dishes for 24 h before treatment with poupartone B (1 µg/mL). Images were acquired every 10 min for 13 h starting immediately after the addition of the drug.

SUPPORTING INFORMATION

MDA-MB-231 cells were treated with increasing concentrations of poupartone B (0.5-2 µg/mL) or vehicle only. Phase-contrast timelapse images of the different culture conditions after 0, 6, 12, 24, 36, and 48 h of treatment are illustrated in Fig. 1S (Supporting Information). A2058 cells were treated with increasing concentrations of poupartone B (0.5-2 µg/mL) or vehicle only. Phase-contrast time-lapse images of the different culture conditions after 0, 6, 12, 24, 36, and 48 h of treatment are illustrated in Fig. 2S (Supporting Information). A375 cells were treated with increasing concentrations of poupartone B (0.5-2 µg/mL) or vehicle only. Phase-contrast time-lapse images of the different culture conditions after 0, 6, 12, 24, 36, and 48 h of treatment are illustrated in Fig. 3S (Supporting Information). Fibroblasts were treated with increasing concentrations of poupartone B (0.5-2 µg/mL) or vehicle only. Phase-contrast time-lapse images of the different culture conditions after 0, 6, 12, 24, 36, and 48 h of treatment are illustrated in Fig. 4S (Supporting Information).

Published in : Planta Med (2021), vol. 87, n°12-13, pp. 1008–1017
DOI: 10.1055/a-1532-2384
Status : Postprint (Author's version)

MDA-MB-231, A2058, A375, normal fibroblasts, HL-60, and OCI-LY19 cells were treated with increasing concentrations (0- 2 µg/mL) of poupartone B, and live-cell imaging was used to mea-sure the relative cell confluency. The areas under the relative cell confluency versus time curves (AUC) are plotted for each concentration tested. Dose-response curves (gray curves) were fitted using the inhibitory concentration versus response-variable slope (4 parameters) function of Graphpad Prism. A representative experiment is illustrated in Fig. 5S (Supporting Information).

MDA-MB-231 cells were exposed to poupartone B (1 µg/mL), and time-lapse imaging by holo-tomographic microscopy was performed for 13 h; the video is available as Supporting Information.

CONTRIBUTORS' STATEMENT

Data collection: AL, BD, LM, DP, DF; design of the study: AL, OJ, MF, EM; statistical analysis: AL, BD, LM, DF, OJ, MF, EM; analysis and interpretation of the data: AL, BD, LM, DP, DF, EM; drafting the manuscript: AL, BD, DP, DF, MF, OJ; critical revision of the manuscript: LM, DP, OJ, MF, EM.

ACKNOWLEDGEMENTS

This work was supported by grants from the Fonds de la Recherche Scientifique-FNRS (F. R. S.-FNRS, Belgium); the Fondation contre le Cancer (Foundation of Public Interest, Belgium); the Fonds Spéciaux de la Recherche (University of Liège); the Fondation Hospitalo Universitaire Léon Fredericq (FHULF, University of Liège); the "Direction Générale Opérationnelle de l'Economie", de l'Emploi et de la Recherche from the Service Public de Wallonie (SPW, Belgium); the Walloon Region through the FRFS-WELBIO strategic research programme; and the Wallonia-Brussels Federation (grant for concerted research actions). DB is the recipient of a FNRS-Télévie grant. EM is a research associate from the Fund for Scientific Research (FNRS, Belgium). This research was also supported by the European Commission and the Regional Council of Reunion Island: Activités Therapeutiques, Cosméologiques et Nutraceutiques de Molécules Issues de la Biodiversité Terrestre, Marine et Microbienne de la Zone Sud-Ouest de l'Ocean Indien (BIOMOL-TCN program), and European Regional Development Fund (ERDF). The authors thank Thibault Courtheoux for the 3D cell imager analysis (Nanolive SA).

CONFLICT OF INTEREST

The authors declare that they have no conflict of interest.

REFERENCES

[1] Ledoux A, St-Gelais A, Cieckiewicz E, Jansen O, Bordignon A, Illien B, Di Giovanni N, Marvilliers A, Hoareau F, Pendeville H, Quetin-Leclercq J, Frédérich M. Antimalarial activities of alkyl cyclohexenone derivatives isolated from the leaves of *Poupartia borbonica*. J Nat Prod 2017; 80: 1750-1757

[2] Otto A, Porzel A, Schmidt J, Brandt W, Wessjohann L, Arnold N. Structure and absolute configuration of pseudohygrophorones A 12 and B 12, alkyl cyclohexenone derivatives from *Hygrophorus abieticola* (Basidiomy-cetes). J Nat Prod 2016; 79: 74-80

[3] Roumy V, Fabre N, Portet B, Bourdy G, Acebey L, Vigor C, Valentin A, Moulis C. Four anti-protozoal and anti-bacterial compounds from *Tapirira guianensis*. Phytochemistry 2009; 70: 305-311

[4] David JM, Chavez JP, Chai HB, Pezzuto JM, Cordell GA. New cytotoxic compounds from *Tapirira guianensis*. J Nat Prod 1998; 61: 287-289

[5] Correia SDJ, David JM, David JP, Chai HB, Pezzuto JM, Cordell GA. Alkyl phenols and derivatives from *Tapirira obtusa*. Phytochemistry 2001; 56: 781-784

[6] Okoth DA, Akala HM, Johnson JD, Koorbanally NA. Alkyl phenols, alkenyl cyclohexenones and other phytochemical constituents from *Lannea rivae* (chiov) Sacleux (Anacardiaceae) and their bioactivity. Med Chem Res 2016; 25: 690-703

[7] Yaouba S, Koch A, Guantai EM, Derese S, Irungu B, Heydenreich M, Yenesew A. Alkenyl cyclohexanone derivatives from *Lannea rivae* and *Lannea schweinfurthii*. Phytochem Lett 2017; 23: 141-148

[8] Hafner M, Niepel M, Chung M, Sorger PK. Growth rate inhibition metrics correct for confounders in measuring sensitivity to cancer drugs.

Published in : Planta Med (2021), vol. 87, n°12-13, pp. 1008–1017
DOI: 10.1055/a-1532-2384
Status : Postprint (Author's version)

Nat Methods 2016; 13: 521-527

[9] Reuven N, Adler J, Meltser V, Shaul Y. The Hippo pathway kinase Lats2 prevents DNA damage-induced apoptosis through inhibition of the tyrosine kinase c-Abl. Cell Death Differ 2013; 20: 1330–1340

[10] Schonn I, Hennesen J, Dartsch DC. Cellular responses to etoposide: cell death despite cell cycle arrest and repair of DNA damage. Apoptosis 2010; 15: 162–172

[11] Iorio F, Knijnenburg TA, Vis DJ, Bignell GR, Menden MP, Schubert M, Aben N, Gonçalves E, Barthorpe S, Lightfoot H, Cokelaer T, Greninger P, van Dyk E, Chang H, de Silva H, Heyn H, Deng X, Egan RK, Liu Q, Mironenko T, Mitropoulos X, Richardson L, Wang J, Zhang T, Moran S, Sayols S, Soleimani M, Tamborero D, Lopez-Bigas N, Ross-Macdonald P, Esteller M, Gray NS, Haber DA, Stratton MR, Benes CH, Wessels LFA,Saez-Rodriguez J, McDermott U, Garnett MJ. A landscape of pharmacogenomic interactions in cancer. Cell 2016; 166: 740–754

[12] Sperandio S, Poksay KS, Schilling B, Crippen D, Gibson BW, Bredesen DE. Identification of new modulators and protein alterations in non-apoptotic programmed cell death. J Cell Biochem 2010; 111: 1401–1412

[13] Ranjan A, Iwakuma T. Non-canonical cell death induced by p53. Int J Mol Sci 2016; 17: 2068

[14] Lee D, Kim IY, Saha S, Choi KS. Paraptosis in the anti-cancer arsenal of natural products. Pharmacol Ther 2016; 162: 120–133

[15] Mohammad RM, Muqbil I, Lowe L, Yedjou C, Hsu HY, Lin LT, Siegelin MD, Fimognari C, Kumar NB, Dou QP, Yang H, Samadi AK, Russo GL, Spagnuolo C, Ray SK, Chakrabarti M, Morre JD, Coley HM, Honoki K, Fujii H, Georgakilas AG, Amedei A, Niccolai E, Amin A, Ashraf SS, Helferich WG, Yang X, Boosani CS, Guha G, Bhakta D, Ciriolo MR, Aquilano K, Chen S, Mohammed SI, Keith WN, Bilsland A, Halicka D, Nowsheen S, Azmi AS. Broad targeting of resistance to apoptosis in cancer. Semin Cancer Biol 2015; 35: S78–S103

[16] Vasan N, Baselga J, Hyman DM. A view on drug resistance in cancer. Nature 2019; 575: 299–309

[17] Yuan R, Hou Y, Sun W, Yu J, Liu X, Niu Y, Lu JJ, Chen X. Natural products to prevent drug resistance in cancer chemotherapy: a review. Ann N Y Acad Sci 2017; 1401: 19–27